Photoactivated Circularly Polarized Luminescent Organic Radicals in Doped Amorphous Polymer

Pengfei She,[a] Yanyan Qin,[a] Yuxiang Zhou,[b] Xiaokang Zheng,[a] Feiyang Li,*[c] Shujuan Liu,[b] Yun Ma,*[b] Qiang Zhao,*[b] and Wai-Yeung Wong*[a]

[a] Dr. P. She, Dr. Y. Qin, X. Zheng, Prof. W-Y. Wong
Department of Applied Biology and Chemical Technology and Research Institute for Smart Energy. The Hong Kong Polytechnic University, Hung Hom, Hong Kong P. R. China and The Hong Kong Polytechnic University Shenzhen Research Institute, Shenzhen 518057, P. R. China.
E-mail: wai-yeung.wong@polyu.edu.hk

[b] Y. Zhou, Prof. Y. Ma, Prof. Q. Zhao
State Key Laboratory of Organic Electronics and Information Displays & Jiangsu Key Laboratory for Biosensors, Institute of Advanced Materials (IAM) & Institute of Flexible Electronics (Future Technology), Nanjing University of Posts and Telecommunications (NUPT), Nanjing 210023 P. R. China
E-mail: iamyma@njupt.edu.cn; iamqzhao@njupt.edu.cn

[c] F. Li
School of Environmental and Chemical Engineering, Jiangsu University of Science and Technology, Zhenjiang 212100, P. R. China
E-mail: Feiyang, Li, email: lifeiyang@just.edu.cn

Supporting information for this article is given via a link at the end of the document.

Abstract: Luminescent organic radicals, especially those with photoactivated circularly polarized luminescence (CPL) features, hold great significance for cutting-edge optoelectronic applications, but their development still remains a challenge. In this study, we propose a novel strategy to achieve photoactivated CPL radicals by bonding two phosphine centers within an axial chiral system, yielding a compound of *R/S*-5,5-bis(diphenylphosphino)-4,4'-bibenzo[d][1,3]dioxole (*R/S*-BDP). The photoactivated *R/S*-BDP molecules in polymer matrix display a robust quantum yield of 19.8% and a dissymmetry factor of 1.2×10^{-4}, marking this work as the first example of photoactivated CPL radicals. Experimental and theoretical analyses reveal that *R/S*-BDP molecules, endowed with double phosphine cores in axial chirality, offer a direct way for intramolecular electron transfer upon photoirradiation. This leads to the generation of radical ionic pairs, which subsequently trigger the donor-acceptor arrangement through intermolecular electron transfer, thereby resulting in stable radical emission. Ultimately, the distinctive photo-responsive CPL radical luminescence has been successfully used for information displays and anti-counterfeiting.

Over the past few decades, luminescent organic radicals have drawn considerable attention as a notable class of emitters, attributed to their unique unpaired electron and doublet emission characteristics,[1-7] enabling them to achieve nearly 100% internal quantum efficiency in electroluminescence. Such a feature has not only demonstrated substantial potential in advancing high-performance organic light-emitting diodes but also paved the way for innovation in various photonic applications, including bioimaging,[8] sensing,[9-12] and information encryption.[13] In light of this, there has been remarkable progress in developing luminescent organic radicals with high quantum efficiency and different emission colors.[14-17] Among them, particularly noteworthy are stimuli-responsive luminescent organic radicals,[18-19] which possess the advantages of rapidly, conveniently, and efficiently tuning luminescence when exposed to various external stimuli, indicating a potentially bright future in cutting-edge photonic applications. Nevertheless, reports on external stimuli-responsive luminescent organic radicals remain scarce.

Recently, triphenylphosphine derivatives have emerged as promising candidates for photoactivated emissive organic radicals.[20,21] These molecules can generate luminescent radicals upon UV irradiation, owing to the formation of phosphorus-centered radicals. This formation results from photoinduced electron transfer (PET) process between adjacent molecules and is followed by pivotal electron separation and stabilization within an intermolecular donor-acceptor (D-A) arrangement (Figure 1a). Nonetheless, the emission of such triphenylphosphine-based radicals has been confined to those arising from the crystalline state. This limitation arises because compact molecular packing and robust intermolecular interactions are imperative to facilitate efficient PET between adjacent molecules. Consequently, confining such radical. emission to crystals substantially impedes their practical applications and processability. Thus, developing luminescent radicals in the film or solution state becomes fundamentally important.

Additionally, current research efforts in this area have aimed to extend the additional dimension of optical signals of luminescent organic radicals to further advance frontier photonic applications.[22-24] Integrating circularly polarized luminescence (CPL) into photoactivated luminescent organic radicals presents an effective method to expand the dimensions of their optical signals. However, considering the intrinsic difficulties in generating luminescent organic radicals upon photoirradiation and achieving efficient charity transfer from chiral groups to organic radicals for CPL within an organic molecule, attaining an organic radical with verified g_{lum} in a solid state remains unprecedented. If photoactivated CPL organic radicals could be

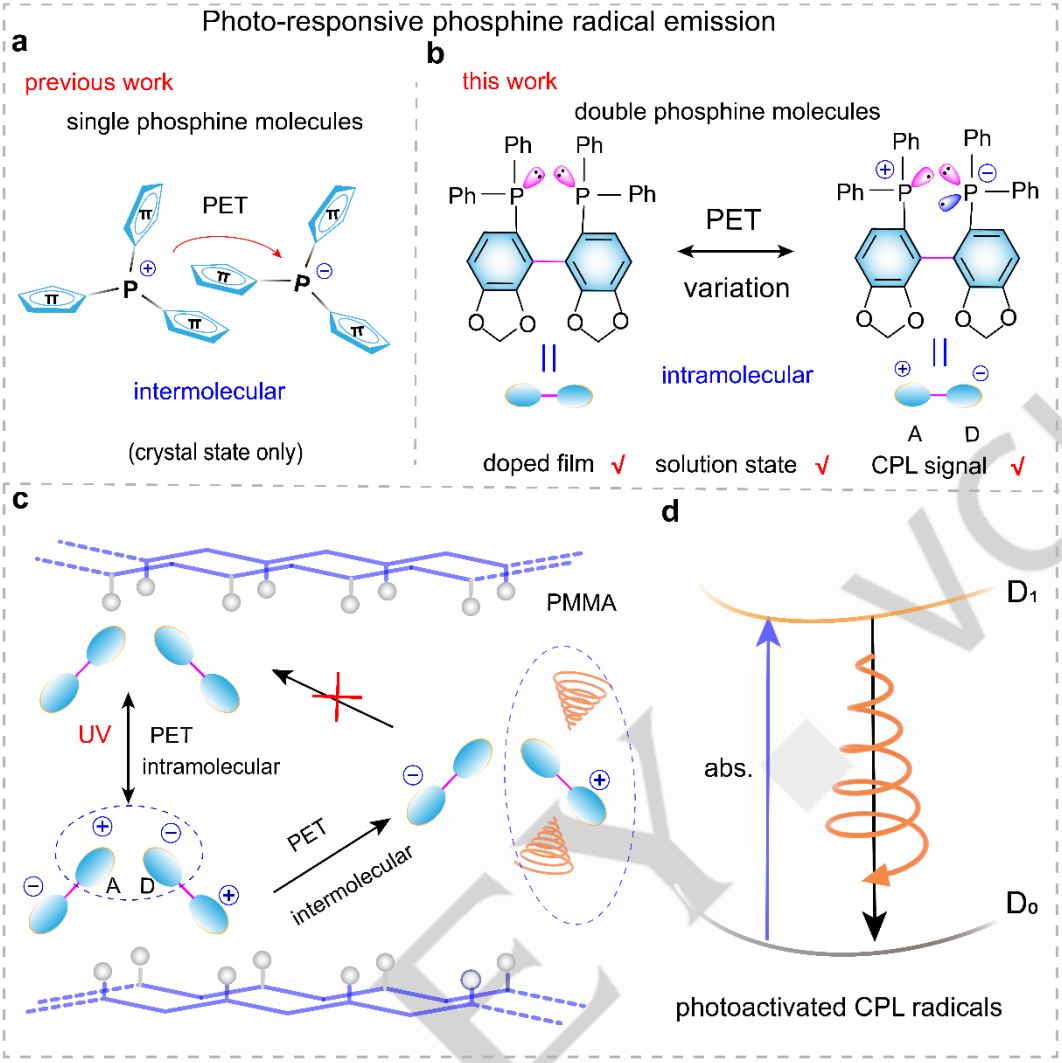

Figure 1. a, b) Schematic design of axial chiral molecules, predicated on a double-phosphine base, facilitating intramolecular electron transfer for D-A conformation. c, d) Proposed mechanism of the photoactivated CPL radical in polymer matrix.

effectively utilized, the variation in chiro-optical properties under light stimuli could serve as an additional monitoring parameter—besides luminescence intensity or color—thus benefiting their practical applications, especially in anti-counterfeiting and information encryption.[25-26]

In this work, we aimed to address aforementioned challenges and realize photoactivated CPL radical in the thin-film and solution state by connecting two phosphine centers in an axial chiral system. This strategy not only facilitates the realization of intramolecular PET processes under photoirradiation but also enables the production of emissive radical with CPL property (Figure 1b). To validate our hypothesis, molecules of *R/S*-5.5-bis(diphenylphosphino)-4,4'-bibenzo[d][13]dioxole (*R/S*-BDP), which incorporate two triphenylphosphine centres within a single axial chiral molecule, were designed (Figures S1-7 and Table S1). By incorporating dioxole units as donors and phenylphosphine units as acceptors, the symmetric architecture is disrupted, providing the vital prerequisite for effective PET between the two phenylphosphine units and subsequently generating emissive radicals through an intermolecular D-A arrangement. As expect, this hybrid intra- and inter-molecular electron transfer allows the persistence of luminescent radical in doped film and solution. Additionally, the intrinsic structural features of axial chiral molecules with adjacent conjugation units enabled the realization of the first example of photoactivated CPL radical within this system (Figures 1c and d). Finally, we explored the potential applications of the unique photoactivated CPL properties of *R/S*-BDP in information displays and anti-counterfeiting.

Commercially obtained *R/S*-5.5-bis(diphenylphosphino)- 4,4'-bibenzo[d][13]dioxole (*R/S*-BDP) were subjected to multiple column chromatography and recrystallization before use. The purified molecules were characterizd *via* ^{1}H, ^{13}C, and ^{31}P nuclear magnetic resonance (NMR) spectroscopy, as well asmatrix-assisted laser desorption/ionization time of flight mass spectrometry (MALDI-TOF-MS). Single crystals of *R/S*-BDP were successfully obtained from a dichloromethane/n-hexane mixture, and the single crystal analysis revealed that two

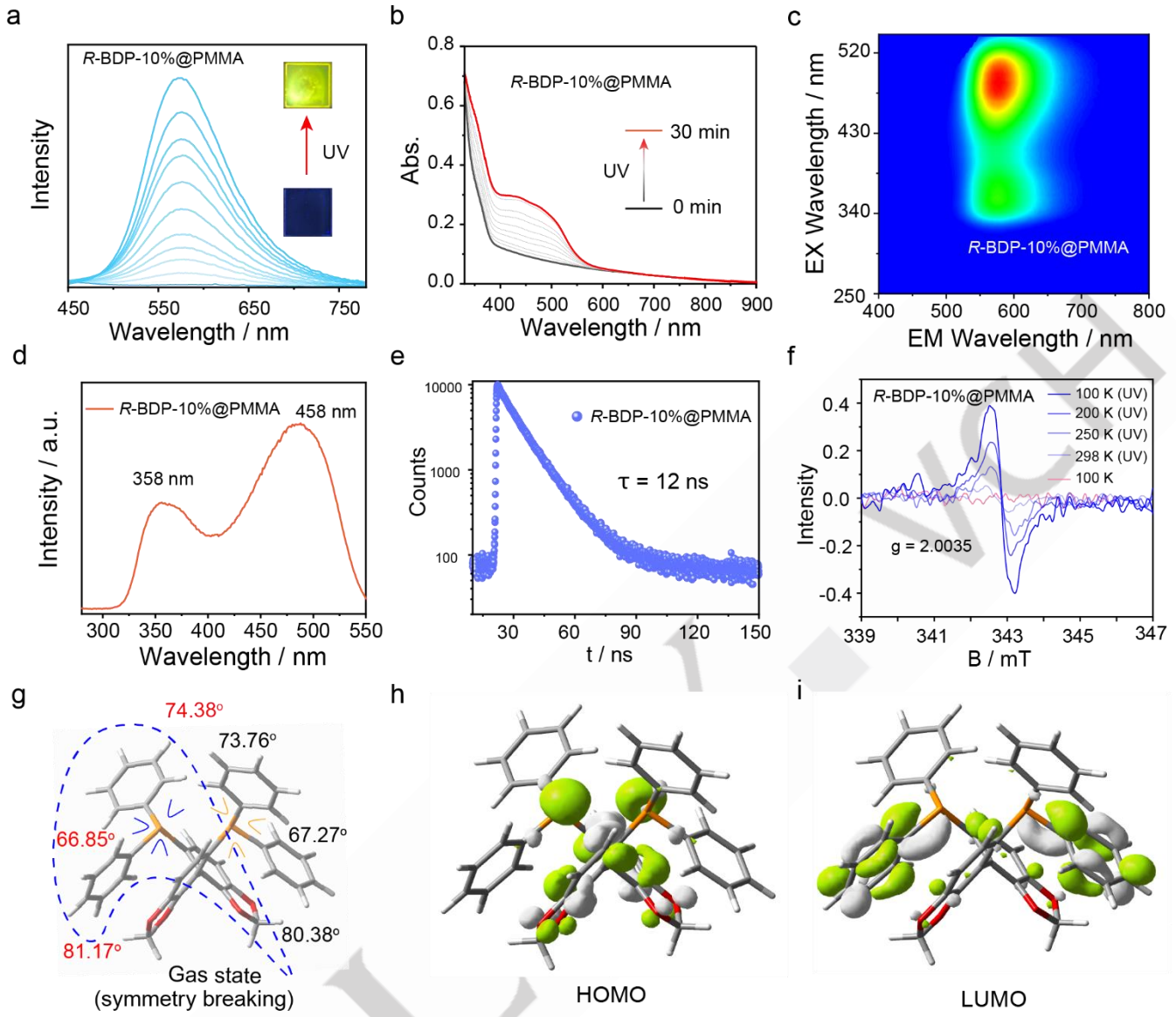

Figure 2. a, b) PL and absorption spectra of *R*-BDP-10%@PMMA, showcasing variations across different photoactivation durations from 0 to 30 mins. c-e) Mapping of excitation-photoluminescence, excitation spectrum and lifetime decay profiles (575 nm) of photoactivated *R*-BDP-10%@PMMA, recorded under ambient conditions at 298 K. f) Electron paramagnetic resonance (EPR) spectra of *R*-BDP-10%@PMMA, captured before and after photoirradiation. g) Depiction of the optimized molecular conformation of *R*-BDP in a gas phase. h, i) Illustrations showcasing electron cloud distributions of *R*-BDP in a gaseous state.

benzo[d][1,3]dioxol-5-yldiphenylphosphane (DP) units possessed an axial skeleton with a dihedral angle of 77.3° or 78.8°. Despite partial interruption of the entire axial enantiomer by the sizable dihedral angle, the distance between two phosphane centers was approximately 3.66 or 3.65 Å (Figure), a distance sufficiently short to ensure their efficient intramolecular PET. This result affirmed the superiority of the dual phosphine centers in the design strategy for axial photoirradiation-induced luminescent radical.

R/S-BDP doped polymethyl methacrylate (PMMA) films with a 10% concentration were prepared through a straightforwarddrop-casting approach, subsequently, investigating their photophysical properties in detail. Firstly, an *R*-BDP doped PMMA film with a 10.0% doping concentration (*R*-BDP-10%@PMMA) was utilized to study its photoactivated luminescence behavior. The photoluminescence (PL) spectra and corresponding photographs revealed a negligible luminescence signal at the initial state, while a bright orange emission at approximately 575 nm gradually increased upon continuous UV irradiation (Figure 2a). Simultaneously, two absorption bands, ranging from 330-400 nm and 400-600 nm, progressively enhanced upon UV irradiation (Figure 2b), a phenomenon also was observable in the excitation spectrum post-UV irradiation (Figures 2c and d), implying the generation of new species. After a photoirradiation duration of 30 min, the enhancement of emission intensity ceased, with the luminescence quantum yield (PLQY) and lifetime at 575 nm measured to be 18.1% and 12 ns, respectively

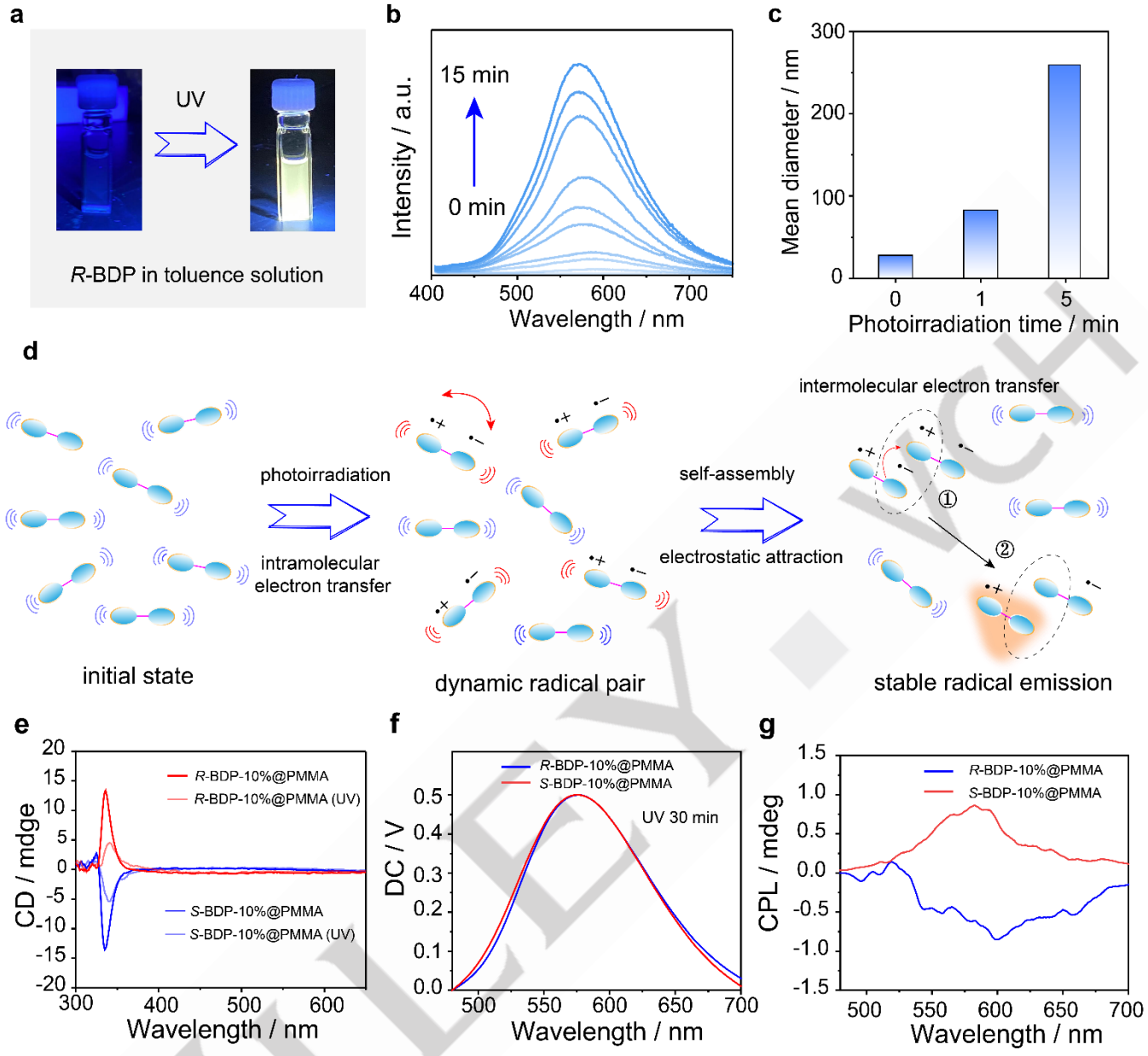

Figure 3. a) Comparative photographs of *R*-BDP in degassed toluene before and after photoactivation under N_2 condition. b) PL spectra of *R*-BDP in toluene, subjected to varying durations of photoirradiation. c) Dynamic light scattering analyses for *R*-BDP in toluene (2×10^{-4} M), both before and after UV irradiation. d) The hypothesized mechanism underpinning the photoactivated CPL radical in toluene. e-g) Comparative circular dichroism (CD) and CPL spectra of *R*/*S*-BDP-10%@PMMA, before and after-photoirradiation.

(Figure 2e and Table S2). Additionally, *R*/*S*-BDP doped PMMA films at varying concentrations (1.0%, 5.0%, 15.0%, and 20.0%) exhibit similar photoirradiation-induced emission behaviors, with *R*-BDP-20%@PMMA showcasing the highest PLQY at 19.8% (Figure S9 and Table S2). Besides, the stability of *R*-BDP-10%@PMMA is remarkable, as the luminescence signal remains almost unchanged for over one week at dark condition (Figure S10).

To reveal the underlying mechanism of the photoactivated luminescence of *R*/*S*-BDP films, a series of control experiments were carried out. At first, ^{1}H NMR spectra of *R*-BDP-10%@PMMA were collected under different UV irradiation time. As depicted in Figure S11, minimal variation is observed in these NMR spectra, suggesting that the molecular structure of *R*-BDP remains intact. Subsequently, electron paramagnetic resonance (EPR) spectroscopy was measured on the *R*-BDP-10%@PMMA film. Figure 2f shows a notable radical signal with a *g* value of 2.0035 after UV irradiation, which is further amplified at lower temperatures. This recorded *g* value aligns with previously reported values associated with persistent phosphine radical cations and radical anions.[20,21] Consequently, we speculate that radical ion pairs may form in *R*/*S*-DBP molecules *via* electron transfer between two intramolecular phosphine atoms. This would subsequently facilitate the regulation of intermolecular D-

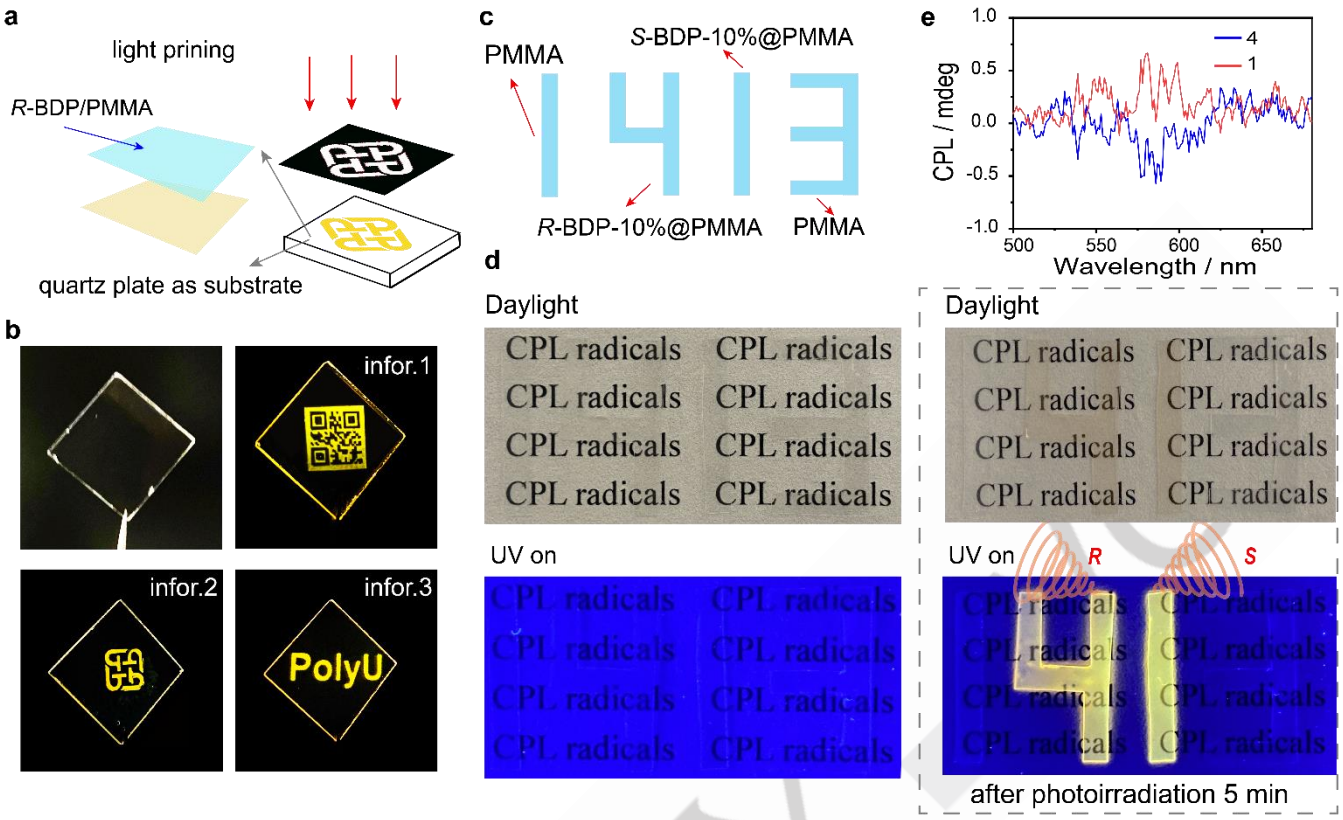

Figure 4. a) Utilization of masked UV irradiation for image production. b) Sequentially inscribed luminescence images on a single transparent substrate. c, d) Visual representation illustrating the process of information encryption and decryption employing both PMMA and R/S-BDP doped PMMA films.

A arrangements in *R*/*S*-BDP molecules, thereby stabilizing phosphine radical emission.

In order to validate our hypothesis, theoretical calculations were conducted to assess the optimized molecular conformation of *R*-BDP in the gas phase, given that symmetry breaking is crucial for generating photoinduced phosphine radicals. As illustrated in Figure 2g, the optimized *R*-BDP conformation displays varying dihedral angles of the phenyl rings within both triphenylphosphine segments, thereby indicating the presence of symmetry breaking. Additionally, the highest occupied molecular orbitals (HOMOs) are predominantly located on the donor moiety of the benzo[d][1,3]dioxole group and the phosphonium core (Figure 2h), whereas the lowest unoccupied molecular orbitals (LUMOs) span across the adjacent phenyl rings (Figure 2i). This notable charge transfer characteristic substantiates the PET between the two phosphine units, resulting in the formation of an intramolecular radical ionic pair. This can be perceived as an enhanced D-A conformation, which effectively facilitates the intermolecular D-A arrangement and electron transfer within amorphous polymers.

To verify the presence of intramolecular radical ionic pairs, we investigated the aggregation behaviors and photophysical properties of *R*-BDP in degassed toluene, motivated by the understanding that intramolecular radical ion pairs can induce electrostatic attraction. This attraction, occurring between the anion moiety of one molecule and the cation region of another, drives the aggregation of *R*-BDP molecules in a D-A arrangement manner. Notably, *R*-BDP in toluene exhibits photoactivated orange emission behavior (Figure 3a), and analogous to the *R*-BDP-10%@PMMA film, parallel variations in absorption and PL spectra are observed upon UV irradiation (Figures 3b and S12). Distinct nanoscale aggregates become observable under varying UV irradiation times (Figures 3c and S13). Moreover, the photoactivated luminescent behavior of *R*-BDP solution persists even at a low concentration (1.0×10^{-6} mol/L), likely attributable to the aggregation driven by electrostatic attraction in D-A aggregates (Figures 3d and S14). Besides, these BDP aggregates not only well confine molecular motion but also enhance electron transfer between molecules, resulting in a bright and stable radical emission in toluene solution. In contrast, no substantial luminescence signal is observed in the photoactivated *R*-BDP-0.2%@PMMA film because the molecules are constrained within the PMMA film, rendering the distance too far to facilitate the regulation of intermolecular D-A arrangement (Figure S9c). The findings well elucidate that within the structured environment of the PMMA matrix, the BDP singlet molecule demonstrates limited electron transfer to neighboring molecules at lower doping concentrations. These results underline the critical role that the proximity between adjacent molecules plays in generating radical emission.

To delve deeper into the mechanism behind photoactivated radical emission, we simulated the absorption spectra of *R*-BDP radical cation and anion using time-dependent density functional theory (TD-DFT). As illustrated in Figure S15, the optimized *R*-

BDP radical cation and anion present distinct absorption bands, aligning consistently with experimental data. It is noteworthy that the absorption band of the BDP radical, within the wavelength range of 350-500 nm, bears a similarity to the excitation spectra of both activated BDP solution and doped film. Consequently, this photoactivated emission could be attributed to the emission of BDP radical cation. For comparative purposes, the DP molecule, representing half of the BDP molecular structure was synthesized (Figures S16-18). Intriguingly, after 30 minutes of photoirradiation, no photoactivated emission behavior is discernible in its solution, doped film, or inherent liquid state (Figure S19), highlighting the pivotal role that double phosphine atoms play in facilitating photoactivated radical emission within the doped amorphous polymer system.

After affirming the photoactivated luminescence behaviors of *R/S*-BDP@PMMA films, we proceeded to examine their chiroptical properties through recording the circular dichroism (CD) and CPL spectra. Figure 3e reveals that the CD spectra of the *R/S*-BDP-10%@PMMA films showcase a commendable mirror-image relationship, evidenced by the positive and negative Cotton effects observed approximately at 336 nm. Subjecting the films to UV irradiation for 30 minutes led to a mild red shift in CD signals at 342 nm and introduced a faint tail band within the 349-395 nm range. Notably, the CPL spectra present conspicuous mirror-image CPL profiles (Figures 3f and g), aligning with a similar trend observed in their PL spectra. Simultaneously, a dissymmetric factor of 1.2×10^{-4} was attained from the photoactivated *R/S*-BDP-10%@PMMA films (Figure S20), thereby confirming the photoirradiation induced CPL behaviors.

Given the distinctive photoactivated CPL radical and the excellent processability features of the *R/S*-BDP thin film system, we explored its potential applications, particularly in the areas of information displays and anti-counterfeiting. Figure 4a illustrates a straightforward display thin film, crafted by utilizing a two-layer structure. Upon mask illumination with UV light, the radical sample was activated, enabling the printing and displaying of diverse patterns on these thin films, as visualized in Figure 4b. Additionally, we harnessed their responsive CPL features to devise high-level information encryption. Figure 4c depicts an encryption pattern “1413,” crafted using pure PMMA (for digits 1 and 3), *R*-BDP-10%@PMMA (4), and *S*-BDP-10%@PMMA (1), respectively. Initially, under daylight and UV light, no distinction could be observed amongst these digits. However, after a 5-minute UV irradiation, the central digits “41” displayed a similar bright yellow emission, but distinct CPL signals were detected from “4” and “1” respectively, as seen in Figures 4d and e. Consequently, the covert correct digit was successfully deciphered. This result highlights the outstanding advantages of the photoactivated CPL radical for high-level information storage and flexible display, markedly enhancing its practical applications in flexible and printed electronics.

In summary, we have proposed an effective strategy to realize photoactivated CPL radical in both amorphous thin films and solution state. Our experimental and theoretical results highlight that *R/S*-BDP molecules with double phosphine cores in an axial chiral structure can provide a direct channel for intramolecular electron transfer upon photoirradiation, leading to the formation of radical ionic pairs. Subsequently, these radical ionic pairs trigger the D-A arrangement via intermolecular electron transfer, resulting in stable radical emission. Noteworthy is that *R/S*-BDP@PMMA films exhibit a remarkable maximum circularly polarized radical emission efficiency of 19.8% at room temperature, and a dissymmetric factor of 1.2×10^{-4} upon UV irradiation. This study provides a blueprint for the design and synthesis of innovative circularly polarized radical materials, marking a pivotal stride in this realm.

Acknowledgements

W.-Y.W. thanks the financial support from the Hong Kong Research Grants Council (PolyU 15301922), the RGC Senior Research Fellowship Scheme (Grant SRFS2021-5S01), the CAS-Croucher Funding Scheme for Joint Laboratories (ZH4A), the ITC Guangdong-Hong Kong Technology Cooperation Funding Scheme (TCFS) (GHP/038/19GD), Miss Clarea Au for the Endowed Professorship in Energy (847S) and Research Institute for Smart Energy (CDAQ) both from the Hong Kong Polytechnic University. This work was also supported by the National Key R&D Program of China (2022YFA1204404), National Natural Science Foundation of China (52073242, 62205277, 61825503 and 62322508).

Conflict of Interest

The authors declare no conflict of interest.

Keywords: photoactivated organic radical, circularly polarized luminescence, double phosphine cores, intramolecular electron transfer, anti-counterfeiting

References:

[1] O. Armet, J. Veciana, C. Rovira, J. Riera, J. Castaner, E. Molins, J. Rius, C. Miravitlles, S. Olivella, J. Brichfeus, *J. Phys. Chem.* **1987**, *91*, 5608-5616.

[2] S S. Gorgon, K. Lv, J. Grüne, B. H. Drummond, W. K. Myers, G. Londi, G. Ricci, D. Valverde, C. Tonnelé, P. Murto, A. S. Romanov, D. Casanova, V. Dyakonov, A. Sperlich, D. Beljonne, Y. Olivier, F. Li, R. H. Friend, E. W. Evans, *Nature* **2023**, *620*, 538-544.

[3] Z. Cui, A. Abdurahman, X. Ai, F. Li, *CCS Chem.* **2020**, *2*, 1129-1145.

[4] B. K. Rugg, M. D. Krzyaniak, B. T. Phelan, M. A. Ratner, R. M. Young, M. R. Wasielewski, *Nat. Chem.* **2019**, *11*, 981-986.

[5] Z. Cui, S. Ye, L. Wang, H. Guo, A. Obolda, S. Dong, Y. Chen, X. Ai, A. Abdurahman, M. Zhang, L. Wang, F. Li, *J. Phys. Chem.* **2018**, *9*, 6644-6648.

[6] Y. Joo, V. Agarkar, S. H. Sung, B. M. Savoie, B. W. Boudouris, *Science* **2018**, *359*, 1391-1395.

[7] C. Shu, Z. Yang, A. Rajca, *Chem. Rev.* **2023**, *123*, 11954–12003.

[8] X. Cui, G. Lu, S. Dong, S. Li, Y. Xiao, J. Zhang, Y. Liu, X. Meng, F. Li, C.-S. Lee, *Mater. Horiz.* **2021**, *8*, 571-576.

[9] S. Chen, Y. Ju, H. Zhang, Y. Zou, S. Lin, Y. Li, S. Wang, E. Ma, W. Deng, S. Xiang, B. Chen, Z. Zhang, *Angew. Chem. Int. Ed.* **2023**, *62*, e202308418.

[10] Y. Hattori, T. Kusamoto, H. Nishihara, *Angew. Chem. Int. Ed.* **2014**, *53*, 11845-11848.

[11] Y. Hattori, S. Kimura, T. Kusamoto, H. Maeda, H. Nishihara, *Chem. Commun.* **2018**, *54*, 615-618.

[12] S. Kimura, A. Tanushi, T. Kusamoto, S. Kochi, T. Sato, H. Nishihara, *Chem. Sci.* **2018**, *9*, 1996-2007.

[13] J.-M. Jin, W.-C. Chen, J.-H. Tan, Y. Li, Y. Mu, Z.-L. Zhu, C. Cao, S. Ji, D. Hu, Y. Huo, H.-L. Zhang, C.-S. Lee, *Angew. Chem. Int. Ed.* **2023**, *62*, e202214281.

[14] M. Lee, I. Song, M. Hong, J. Y. Koo, H. C. Choi, *Adv. Func. Mater.* **2018**, *28*, 1703509.

[15] X. Ai, E. W. Evans, S. Dong, A. J. Gillett, H. Guo, Y. Chen, T. J. H. Hele, R. H. Friend, F. Li, *Nature* **2018**, *563*, 536-540.

[16] Y. Zhao, A. Abdurahman, Y. Zhang, P. Zheng, M. Zhang, F. Li, *CCS Chem.* **2021**, *4*, 722-731.

[17] H. Guo, Q. Peng, X.-K. Chen, Q. Gu, S. Dong, E. W. Evans, A. J. Gillett, X. Ai, M. Zhang, D. Credgington, V. Coropceanu, R. H. Friend, J.-L. Brédas, F. Li, *Nat. Mater.* **2019**, *18*, 977-984.

[18] Y. Li, G. V. Baryshnikov, C. Xu, H. Ågren, L. Zhu, T. Yi, Y. Zhao, H. Wu, *Angew. Chem. Int. Ed.* **2021**, *60*, 23842-23848.

[19] W. Zheng, X. Li, G. V. Baryshnikov, X. Shan, F. Siddique, C. Qian, S. Zhao, H. Wu, *Angew. Chem. Int. Ed.* **2023**, *62*, e202305925.

[20] X. Zhao, J. Gong, P. Alam, C. Ma, Y. Wang, J. Guo, Z. Zeng, Z. He, H. Y. Sung Herman, D. Williams Ian, S. Wong Kam, S. Chen, W. Y. Lam Jacky, Z. Zhao, Z. Tang Ben, *CCS Chem.* **2021**, *4*, 1912-1920.

[21] C. Tang, L. Song, K. Zhou, P. Ren, E. Zhao, Z. He, *Chem. Sci.* **2023**, *14*, 1871-1877.

[22] M. Wang, E. Zhao, Z. He, *ChemPhotoChem* **2023**, e202300101.

[23] P. Mayorga Burrezo, V. G. Jiménez, D. Blasi, I. Ratera, A. G. Campaña, J. Veciana, *Angew. Chem. Int. Ed.* **2019**, *58*, 16282-16288.

[24] S. Kimura, T. Kusamoto, S. Kimura, K. Kato, Y. Teki, H. Nishihara, *Angew. Chem. Int. Ed.* **2018**, *57*, 12711-12715.

[25] Z. Huang, Z. He, B. Ding, H. Tian, X. Ma, *Nat. Commun.* **2022**, *13*, 7841.

[26] Y. Jin, Q.-C. Peng, J.-W. Xie, K. Li, S.-Q. Zang, *Angew. Chem. Int. Ed.* **2023**, *62*, e202301000.